# Tunability of MoO$_3$ Thin-Film Properties Due to Annealing in Situ Monitored by Hard X-ray Photoemission

Xiaxia Liao,[*,†,§] Ah Reum Jeong,[†] Regan G. Wilks,[†,‡] Sven Wiesner,[†] Marin Rusu,[†] Roberto Félix,[†] Ting Xiao,[†] Claudia Hartmann,[†] and Marcus Bär[*,†,‡,¶,∥]

[†]Department Interface Design, Helmholtz-Zentrum Berlin für Materialien und Energie GmbH, Hahn-Meitner-Platz 1, 14109 Berlin, Germany

[§]School of Materials Science and Engineering, Nanchang University, Nanchang 330031, PR China

[‡]Energy Materials In-situ Laboratory Berlin (EMIL) and [¶]Helmholtz-Institute Erlangen-Nürnberg for Renewable Energy (HI ERN), Helmholtz-Zentrum Berlin für Materialien und Energie GmbH, Albert-Einstein-Strasse 15, 12489 Berlin, Germany

[∥]Department of Chemistry and Pharmacy, Friedrich-Alexander-Universität ErlangenNürnberg, Egerlandstrasse 3, 91058 Erlangen, Germany

**S** Supporting Information

**ABSTRACT:** The chemical and electronic structure of MoO$_3$ thin films is monitored by synchrotron-based hard X-ray photoelectron spectroscopy while annealing from room temperature to 310 °C. Color-coded 2D intensity maps of the Mo 3d and O 1s and valence band maximum (VBM) spectra show the evolution of the annealing-induced changes. Broadening of the Mo 3d and O 1s spectra indicate the reduction of MoO$_3$. At moderate temperatures (120−200 °C), we find spectral evidence for the formation of Mo$^{5+}$ and at higher temperatures (>165 °C) also of Mo$^{4+}$ states. These states can be related to the spectral intensity above the VBM attributed to O vacancy induced gap states caused by partial filling of initially unoccupied Mo 4d-derived states. A clear relation between annealing temperature and the induced changes in the chemical and electronic structure suggests this approach as a route for deliberate tuning of MoO$_3$ thin-film properties.
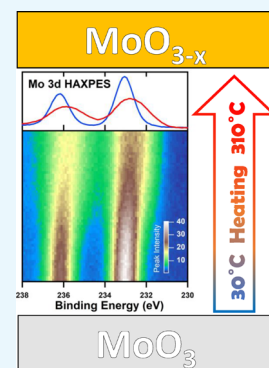
## INTRODUCTION

It has been demonstrated that molybdenum trioxide (MoO$_3$) is an excellent (inorganic) hole transport material (HTM) in optoelectronic devices, such as solar cells and/or organic light-emitting diodes (OLEDs).[1,2] Due to its large work function, MoO$_3$ generally has a favorable energy level alignment with the active materials and the anode in these devices.[3−5] For example, in organic solar cells (OSCs), after replacing the (organic) HTM PEDOT:PSS with inorganic MoO$_3$, mainly to improve long-term stability, the efficiency remained unchanged or was even improved.[6−8] However, for perovskite-based photovoltaic devices, it has been suggested that the deep valence band of MoO$_3$ blocks the hole transport.[9] One proposed solution to overcome this problem is to create states within the band gap above the valence band maximum (VBM), also called gap states.[10] Gap states in MoO$_3$ thin films can be created through, for example, exposure to a reducing atmosphere,[11] ion bombardment,[12] thermal annealing,[13,14] etc. The induced (defect) states in the band gap are suggested to generate conduction paths, enhancing hole extraction.[10] For device optimization, Vasilopoulou et al.[15] studied the correlation between the electronic structure and the composition of MoO$_3$ films and reported the improvements of OSCs and OLEDs performance upon creating oxygen vacancies or inserting hydrogen atoms into the employed

MoO$_3$. A more favorable energy level alignment was suggested as an explanation, reducing voltage loss and facilitating barrier-free hole extraction. Sample annealing treatments are a common way to introduce oxygen vacancies to tune the electronic structure of metal oxides.[16,17] With increasing annealing temperature, defect states are proposed to form due to oxygen escaping from the sample (surface); this process in principle allows deliberate modification of the material's electronic structure. Dasgupta et al.[18] reported a MoO$_3$ annealing temperature of 250 °C in the N$_2$ atmosphere to be ideal, resulting in an improved charge transport yielding a 50% solar cell performance enhancement. In contrast, Lee et al.[19] demonstrated that an annealing-induced reduction of MoO$_3$ is detrimental: They reported a reduced OSC efficiency independent of whether the MoO$_3$ was annealed in N$_2$, mixed H$_2$/N$_2$ atmosphere, or ambient air at 200 or 400 °C, compared to using as-prepared MoO$_3$ films. It was suggested that for the as-prepared MoO$_3$, in this particular case, the intrinsic oxygen vacancies and, thus, the already present gap states provided sufficient hole transport, while annealing led to further reduction and detrimental metallic behavior. Note that
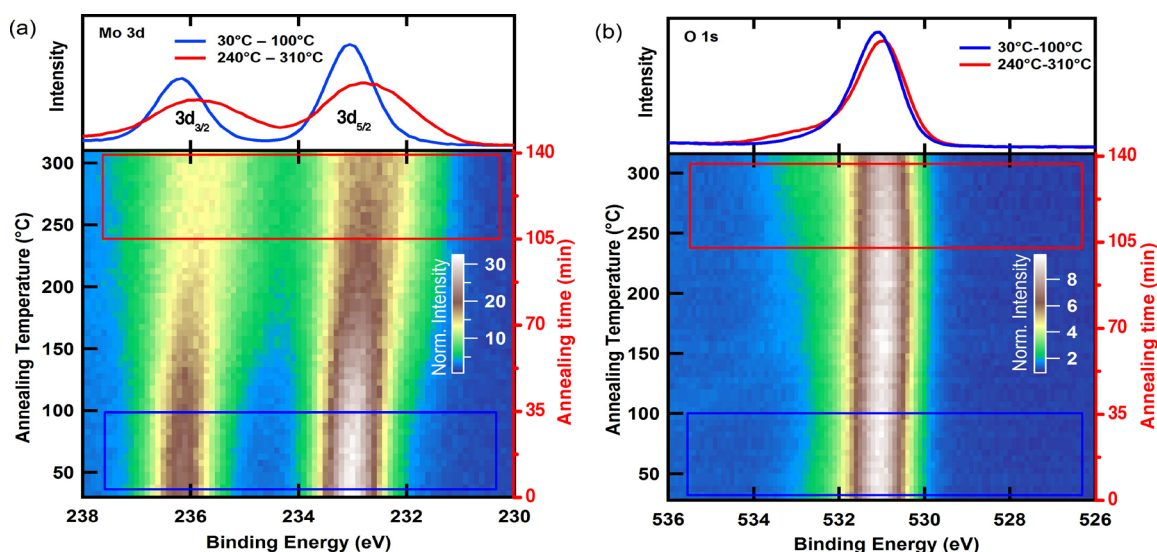
**Figure 1.** Evolution of the (a) Mo 3d and (b) O 1s spectra upon in situ annealing in vacuum presented in 2D intensity maps, where the $x$ axis represents the binding energy region of the spectra, the $y$ axis shows the annealing temperature (and thus also annealing time), and the color code indicates the normalized spectral intensity. The upper panels show respective sum spectra recorded in the stated temperature regime.

in this case, the (surface) stoichiometry can be expected to significantly deviate from the nominal [O]:[Mo] = 3:1 composition. These seemingly inconsistent results might be attributed to the different initial (i.e., as-prepared) states of the studied $MoO_3$ materials in terms of oxygen vacancy/gap state density.

In order to systematically study the impact of annealing on the [O]:[Mo] composition and the presence and density of gap states, we have in situ monitored the changes in the chemical and electronic structure of $MoO_3$ thin films by hard X-ray photoelectron spectroscopy (HAXPES) while annealing in vacuum. This will establish a sound base for the deliberate tuning of the gap states density via the [O]:[Mo] composition in molybdenum oxides.

## RESULTS AND DISCUSSION

The survey spectra of the as-prepared and annealed $MoO_3$ films (i.e., before and after in situ annealing, respectively) are shown in the Supporting Information (see Figure S1). All expected core level lines of Mo and O atoms are detected. In addition, a small C 1s peak can be observed that might indicate the presence of surface contaminants formed on the sample during sample transport (in inert gas) and/or sample mounting (in ambient conditions). Note that the incorporation of (some) carbon in the $MoO_3$ material during PVD processing under high vacuum conditions can also not be excluded. At first sight, the spectra are very similar before and after annealing, for a more detailed discussion of the annealing-induced changes, we will focus on the detail spectra in the following.

In order to better follow the changes of the Mo 3d and O 1s detail spectra during in situ annealing, the individual spectra are summarized as 2D maps in Figure 1a,b, respectively. The $x$ axis shows the BE region of the spectra; the color code indicates the spectral intensity (normalized to the intensity in the BE range of 227.5−228.5 eV for Mo 3d and 524−525 eV for O 1s to exclude intensity variations due to fluctuating photon flux); and the $y$ axis represents the annealing temperature (and thus also annealing time). The 2D maps (in particular of the Mo 3d line) clearly show a redistribution

of spectral intensity indicating annealing-induced changes of the $MoO_3$ chemical structure. However, also distinct spectral changes in the O 1s line (i.e., emergence of peak at BE ∼533.1 eV) induced by the annealing treatment are observed. The top panels in Figure 1 show respective (a) Mo 3d and (b) O 1s sum spectra derived by adding individual spectra in the temperature ranges of 30−100 °C and 240−310 °C.

From RT to around 100 °C (i.e., the temperature range highlighted by the blue box and represented by the blue spectrum in the top panel of Figure 1a), little or no change is detected in the Mo 3d 2D map. Increasing the annealing temperature from 100 °C to around 240 °C, in contrast, causes obvious changes of the Mo 3d spectra. The $3d_{3/2}$ and $3d_{5/2}$ peaks undergo significant asymmetric broadening, and the peaks gradually shift to lower BE values. A further increase of the annealing temperature to 310 °C seems to result only in comparatively minor additional peak broadening. This is somewhat different to what can be observed for the O 1s spectra, here the most pronounced change, indicated by an asymmetric narrowing of the main peak and a broadening of the minor contribution toward high BE values, can be observed for temperatures below 100 °C and above 200 °C, respectively, with only minor changes in the intermediate temperature regime. Overall, the spectral changes are less pronounced for the O 1s, compared to the Mo 3d spectra, but can clearly be observed in the top panel of Figure 1b.

$MoO_3$ is known to suffer X-ray beam-induced changes,[20] however, measurement parameters have been optimized at the beginning of the experiment to minimize these effects. In fact, after this optimization, no indication of beam damage was observed before and after the measurement sequence (see Figure S2) and thus, we clearly attribute the observed redistribution of spectral intensity to the annealing (and not due to X-ray irradiation).

To quantitatively analyze the annealing-induced changes, the individual spectra have been fitted (see Supporting Information for details and Figure S3 for selected fit spectra). For the as-prepared $MoO_3$ film, the spectrum can be reasonably fit by a single spin-orbit doublet (Mo $3d_{5/2}$ located at BE: 232.5 ± 0.05 eV). Thus, the main oxidation state of molybdenum in

our sample is +6,[21] which is in line with a stoichiometric $MoO_3$ film. However, the nonzero residuum of the fit (see top left panel of Figure S3) suggests that the presence of a small amount of lower oxidation state Mo cannot be excluded, in accordance with refs 18 and 22. At 120 °C, an additional doublet located at lower BE (Mo $3d_{5/2}$ at BE: $231.6 \pm 0.05$ eV, see Figure S3) appears, which increases in intensity with annealing temperature. This doublet is ascribed to the +5 oxidation state of Mo.[15] For annealing temperatures above approximately 200 °C, a third doublet (again at a lower Mo $3d_{5/2}$ at BE: $230.7 \pm 0.05$ eV, see Figure S3) is required to properly fit the Mo 3d line, which is ascribed to the Mo oxidation state +4.[23] In Figure S3, it can be observed that the Mo 3d contributions that represent high Mo oxidation states gradually shift to higher BE values with increasing annealing temperature, likely due to the gradual appearance of the additional low oxidation state contributions at lower BE values. At the same time, the spectral intensity of the low oxidation state (i.e., $Mo^{5+}$ and $Mo^{4+}$) contributions increases at the expense of the high oxidation state (i.e., $Mo^{6+}$) components. The most common explanation for the appearance of low Mo oxidation states is the creation of oxygen vacancies and a related charge transfer upon vacuum annealing.[16]

Based on the Mo 3d fits, the $Mo^{x+}/Mo_{total}$ intensity ratios are derived. As shown in Figure 2a, the Mo oxidation state +6
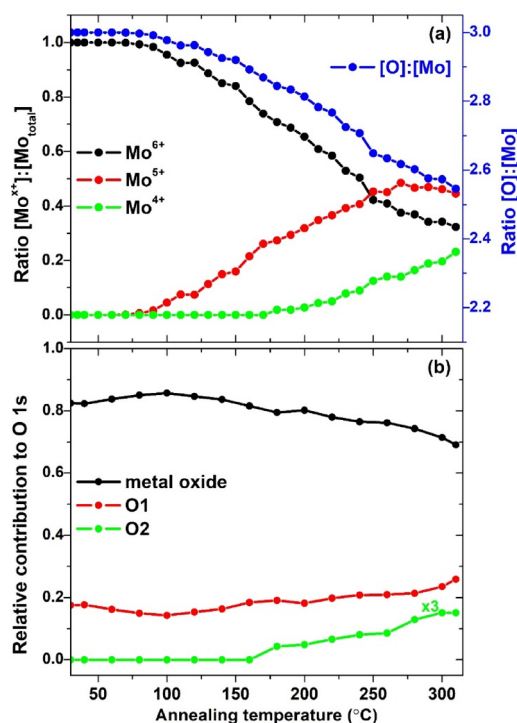


**Figure 2.** (a) $Mo^{x+}/Mo_{total}$ ratios (left y axis) and the [O]:[Mo] ratio (right y axis) and (b) relative contribution to the O 1s line of the studied $MoO_3$ thin films as function of annealing temperature as derived from the data in Figure 1.

contribution decreases with increasing annealing temperature from almost 100% (at RT) to 65.4% (at 200 °C). At the same time, the Mo oxidation state +5 contribution increases, explaining the gradual broadening of Mo 3d spectra in this temperature regime. At even higher annealing temperatures, additional Mo oxidation state +4 contributions can be identified increasing to 23.1% at 310 °C. The fact that the

Mo oxidation state +5 contributions start to plateau at 240 °C, while the slope of the Mo oxidation state +6 contribution decrease is rather constant, indicates that in this temperature region, the reduction process is dominated by the direct +6 → +4 oxidation state conversion or the dynamic balance between the conversion of +6 → +5 and + 5 → +4 oxidation states. Our finding is in agreement with previous reports on $MoO_3$ films annealed in the $N_2$ atmosphere.[23] The degree of reduction can be expressed by the [O]:[Mo] (surface) composition. The [O]:[Mo] ratio derivation is based on the oxidation state contributions to the Mo 3d spectra assuming a [O]:[Mo] = 3 for the oxidation state +6 (i.e., $MoO_3$), [O]:[Mo] = 2.5 for the oxidation state +5 (i.e., $Mo_2O_5$), and [O]:[Mo] = 2 for the oxidation state +4 (i.e., $MoO_2$). From RT to 240 °C, the [O]: [Mo] ratio changes from 3.0 (stoichiometric $MoO_3$) to 2.7 (see blue line in Figure 2a). Note that a similar loss (−10%) of oxygen is derived when the O 1s (Figure S4) and Mo 3d (Figure S3) lines are used for quantification and that our result is similar to that reported by Zhang et al. for annealing in $N_2$. They found that the [O]:[Mo] ratio also decreases from 3.0 to 2.7 when raising the annealing temperature from RT to 250 °C.[23] It is observed that below 100 °C (see Figure 2a), neither the [O]:[Mo] ratio nor the predominant Mo oxidation state +6 changes significantly; most likely because the thermal energy (even in combination with vacuum conditions) is insufficient to break O−Mo bonds.

For the curve fit analysis of the O 1s spectra (see Supporting Information, Figure S4), at low annealing temperature, two spectral components are sufficient to get a reasonable fit. The dominant peak at $530.54 \pm 0.05$ eV is in the BE range that generally can be attributed to metal oxides, that is, $MoO_3$.[15] The smaller high binding energy contribution O1 at $531.69 \pm 0.05$ eV is in a BE range that is usually ascribed to (surface) −OH groups.[15,24] As the temperature increases from RT to approximately 100 °C, it can be observed that the high binding energy contribution gets smaller (see Figure S4 and also indicated by the narrowing of the O 1s peak visible in the 2D map in Figure 1b). Increasing the temperature further, starting from approximately 200 °C, a third contribution (O2) at $533.09 \pm 0.05$ eV is required for a reasonable fit and component O1 increases again. This is accompanied by a widening of the O 1s peak (see 2D map in Figure 1b). While the initial decrease of component O1 with increasing temperature agrees with the attribution to −OH groups (due to annealing-induced dehydration or desorption of surface −OH groups), the subsequent O1 increase at higher temperatures indicates oxygen in another chemical environment. Indeed O 1s contributions of molybdenum oxide in this BE range are also often related to oxygen present in molybdenum suboxides and the related distorted chemical environment due to oxygen vacancies.[13] The spectral fraction of all oxygen components as derived from the spectra in Figure 1b are displayed in Figure 2b. While the O-metal contribution to the O 1s line continuously decreases with annealing temperature, the spectral fraction of O1 shows a shallow minimum around 100 °C and a slight but steady increase at higher temperatures. Thus, at low temperature, we suggest the O1 component of the O 1s line to be mainly due to −OH groups, which dehydrate or desorb with increasing temperature. The increase of the O1 spectral fraction can then be explained by an enhanced presence of molybdenum suboxides (or oxygen vacancies) increasingly formed at temperatures >100 °C. This model is corroborated by the finding of

increased $Mo^{5+}$ at annealing temperatures of 100 °C and higher (see Figure 2a). The onset of increased O2 component intensity of the O 1s line and the appearance of $Mo^{4+}$ in the Mo 3d spectra coincide (see Figure 2a,b), and so, we speculate that the O 1s component O2 can be ascribed to (another) chemical oxygen environment distorted by an even higher amount of oxygen vacancies. The presence of different chemical oxygen environments that appear at different concentrations of oxygen vacancies can be explained as being due to the differing coordination of the oxygen atoms at a molybdenum oxide surface. According to Tokarz-Sobieraj et al.,[25] three types of oxygen exist at the surface of a molybdenum oxide: singly, doubly, and triply coordinated oxygen. The limited surface sensitivity of our HAXPES measurements and relaxation processes at the molybdenum oxide surface upon formation of oxygen vacancies (as suggested in ref 28) can lead to scenarios that would be in agreement with the observed behavior.

The valence band (VB) region (Figure S5) was recorded during the in situ annealing experiment. Due to the low photoionization cross section of the VB states, the data has a significantly lower signal-to-noise ratio than the 2D intensity maps of the Mo 3d and O 1s lines in Figure 1. At first sight, no distinct spectral changes with annealing temperature can be observed. However, close inspection of summations of spectra derived by adding individual spectra in the temperature ranges of 30−100 °C and 240−310 °C depicted as blue and red spectra, respectively, in the top panel of Figure S5, reveals small but significant differences. In the above-VBM region between 0 and 2.8 eV BE, increased spectral intensity can be observed in the high-temperature sum spectrum (red spectrum) compared to the low-temperature sum spectrum (blue spectrum). A detailed evolution of these above-VBM (or gap) states is presented in Figure S6 (left panel). Despite the low signal-to-noise ratio, it seems that these states are not present until the annealing temperature exceeds 165 °C, confirmed by the quantified spectral intensity in the region between 3 and −2 eV (Figure S6, right panel), for which an increase can be identified in spite of considerable variation. At approximately this temperature, we start to find evidence for the presence of Mo in an oxidation state of +4 (see Figure 2a). However, due to the insufficient signal-to-noise ratio (in particular in the above-VBM region) of the data acquired in the fast in situ measurement mode, it is not possible to exclude the presence of above-VBM spectral intensity also for lower annealing temperatures (see discussion below).

High-quality VBM spectra of the as-prepared and annealed $MoO_3$ film recorded before and after the in situ experiment are shown in Figure 3. The individual regions in these spectra are discussed in detail in our previous publication.[20] The majority of the spectral intensity (in particular between BEs of 10 and 2.5 eV) has O 2p character. Under both conditions, the VBM position as derived by linear approximation of the leading edge is determined to be 3.00 ± 0.10 eV below $E_F$ independent of annealing, which is in agreement with VBM values reported for (nearly) stoichiometric $MoO_3$ films.[15] Above-VBM (defect) states in the band gap are detectable but very weak in the as-prepared $MoO_3$ film. Greiner et al. suggested that, from a thermodynamics perspective, even stoichiometric $MoO_3$ can contain some defect concentration.[21] After annealing, two pronounced above-VBM features with local maxima at BE of ~0.8 and ~1.8 eV are detected (indicated by the blue arrows). In transition metal oxides, these (defect) states can generally
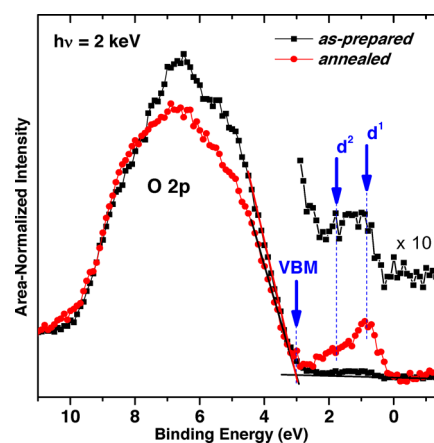


**Figure 3.** High-resolution HAXPES detail spectra of the valence band maximum (VBM) region of the as-prepared and annealed $MoO_3$ thin film. The above-VBM region of the as-prepared $MoO_3$ thin film is also shown on a magnified (×10) scale for comparison. The linear approximation of the leading edges to derive the VBM position is also depicted.

be attributed to the partially filled metal d band (in our case, the usually unoccupied Mo 4d-derived states). However, the origin of these defect states is still under debate. Many studies suggest that oxygen vacancies are the main reason for these defect gap states. Greiner et al.,[16] for example, differentiate between dilute (i.e., low) and nondilute (i.e., very high) O vacancy defect concentration scenarios and attribute $d^1$ and $d^2$ to singly and doubly occupied d bands of $Mo^{5+}$ and $Mo^{4+}$ cations, respectively. While our data of the annealed $MoO_3$ sample seems to agree with the nondilute O vacancy defect concentration scenario, close inspection of the above-VBM region of the as-prepared $MoO_3$ on a magnified (×10) scale in Figure 3, showing spectral intensity in the $d^2$ region, however, contradicts the corresponding dilute O vacancy defect concentration scenario. This points to a more complex explanation. The defect states in $MoO_3$/organic material structures, for example, are typically explained by the charge transfer from the organic materials to the $MoO_3$ film or by interface states, rather than by the intrinsic property of $MoO_3$.[26,27] Additional high-quality spectra of particularly the above-VBM region as a function of O vacancy defect concentration (i.e., $Mo^{x+}/Mo_{total}$ ratio) would be required to ultimately resolve this issue, in the future.

## ■ EXPERIMENTAL SECTION

Thin films of 50 nm $MoO_3$ were deposited onto Au (100 nm)/ glass substrates by physical vapor deposition (PVD) in high vacuum condition (~$10^{-7}$ mbar) as in our previous study of $MoO_3$.[20] For the transport to the analysis tool, the $MoO_3$/Au/ glass samples were sealed in the $N_2$-purged glovebox directly connected to the PVD system.

The HAXPES measurements were conducted at the high kinetic energy photoelectron spectrometer (HiKE) endstation located at the BESSY II KMC-1 beamline at Helmholtz-Zentrum Berlin für Materalien und Energie GmbH (HZB).[28,29] During the sample mounting and loading into the analysis system, air exposure was limited to <10 min. HiKE is equipped with a Scienta R4000 electron energy analyzer and is operated in ultrahigh vacuum (UHV) conditions: base pressure in the analysis chamber is ~$10^{-9}$ mbar. For the HAXPES measurements, the excitation energy was set to 2003

eV (henceforth simply called "2 keV"). The pass energy and energy step width were 200 eV (500 eV) and 0.1 eV (0.5 eV) for all the core levels (survey) scans, respectively. The binding energy (BE) scales of the HAXPES spectra were calibrated using Au 4f reference measurements of a clean Au foil, setting the Au $4f_{7/2}$ core level line to be at 84.00 eV. The total energy resolution of the core level spectra was approximately 0.25 eV. The inelastic mean free path of the photoelectrons depends on their kinetic energy and is around 3 nm in $MoO_3$ for the considered photoemission lines and excitation energy, that is, the signal contribution exponentially decreases to <5% for 8 nm (for the O 1s line) and 10 nm (for the valence band) from the sample surface for the measurement geometry used here.[30,31]

First, high-quality HAXPES data were taken on the as-prepared $MoO_3$ film. Then, the O 1s, Mo 3d, shallow core level, and valence band energy regions were measured consecutively in a fast in situ measurement mode while heating the sample at a rate of approximately 2 °C/min in UHV, covering a temperature (pressure) range from 25 °C ($\sim 10^{-9}$ mbar) up to 310 °C ($\sim$low $10^{-7}$ mbar range) as measured by a type N (Nicrosil-Nisil) thermocouple connected to the sample stage. This in situ annealing was controlled by a resistive heater controller (ZRHCN RHC, Vacuum Generator) unit, which regulates the current applied to the resistive heater below the sample stage based on the thermocouple feedback. For the acquisition of one Mo 3d spectrum, the total measurement time is 36 s. Because the heating rate is rather slow (2 °C/min), we consider the change in temperature over the course of the collection of one spectrum to be negligible. Data acquisition continued after turning off the heater until the sample cooled down to room temperature. Finally, a full set of high-quality HAXPES data of the annealed $MoO_3$ sample was collected. Note that at this point, the [O]:[Mo] composition does significantly deviate from the 3:1 stoichiometry of the as-prepared $MoO_3$. We will nevertheless refer to this sample as "annealed $MoO_3$" in the following.

## CONCLUSIONS

In this work, the chemical and electronic structure of $MoO_3$ thin films has been in situ monitored by hard X-ray photoelectron spectroscopy during vacuum annealing. The VBM position was found to be independent of annealing at $3.00 \pm 0.10$ eV below $E_F$. However, broadening of the Mo 3d and O 1s spectra with increasing annealing temperature is attributed to the formation of $Mo^{5+}$ and (for >165 °C) $Mo^{4+}$ states. At the same time the [O]:[Mo] ratio decreases from 3.0 to 2.7. As a consequence of the significant annealing-induced formation of $Mo^{5+}$ and $Mo^{4+}$, an increasing above-VBM spectral intensity can be observed attributed to O vacancy related gap states due to partial filling of (initially unoccupied) Mo 4d-derived states. Therefore, vacuum annealing is suggested as a simple approach to deliberately tune the properties of $MoO_3$ thin films.

## ASSOCIATED CONTENT

### Ⓢ Supporting Information

The Supporting Information is available free of charge on the ACS Publications website at DOI: 10.1021/acsomega.9b01027.

Survey spectra, impact of X-ray irradiation, curve fit results, evolution of the HAXPES spectra around the valence band maximum (VBM), and the summed up VBM spectra (PDF)

## ■ AUTHOR INFORMATION

### Corresponding Authors
*E-mail: liaoxiaxia8816@163.com (X.L.).
*E-mail: marcus.baer@helmholtz-berlin.de (M.B.).

### ORCID
Xiaxia Liao: 0000-0003-2796-5729
Roberto Félix: 0000-0002-3620-9899
Claudia Hartmann: 0000-0002-8017-8161
Marcus Bär: 0000-0001-8581-0691

### Notes
The authors declare no competing financial interest.

## ■ REFERENCES

(1) Meyer, J.; Hamwi, S.; Kröger, M.; Kowalsky, W.; Riedl, T.; Kahn, A. Transition Metal Oxides for Organic Electronics: Energetics, Device Physics and Applications. *Adv. Mater.* **2012**, *24*, 5408−5427.

(2) Wang, C.; Irfan, I.; Liu, X.; Gao, Y. Role of molybdenum oxide for organic electronics: Surface analytical studies. *J. Vac. Sci. Technol., B: Nanotechnol. Microelectron: Mater., Process., Meas., Phenom.* **2014**, *32*, No. 040801.

(3) Kim, D. Y.; Subbiah, J.; Sarasqueta, G.; So, F.; Ding, H.; Irfan; Gao, Y. The effect of molybdenum oxide interlayer on organic photovoltaic cells. *Appl. Phys. Lett.* **2009**, *95*, No. 093304.

(4) Meyer, J.; Shu, A.; Kröger, M.; Kahn, A. Effect of contamination on the electronic structure and hole-injection properties of MoO3/organic semiconductor interfaces. *Appl. Phys. Lett.* **2010**, *96*, 133308.

(5) Yi, Y.; Jeon, P. E.; Lee, H.; Han, K.; Kim, H. S.; Jeong, K.; Cho, S. W. The interface state assisted charge transport at the MoO3/metal interface. *J. Chem. Phys.* **2009**, *130*, No. 094704.

(6) Liu, J.; Shao, S.; Fang, G.; Meng, B.; Xie, Z.; Wang, L. High-Efficiency Inverted Polymer Solar Cells with Transparent and Work-Function Tunable MoO3-Al Composite Film as Cathode Buffer Layer. *Adv. Mater.* **2012**, *24*, 2774−2779.

(7) Murase, S.; Yang, Y. Solution Processed MoO3 Interfacial Layer for Organic Photovoltaics Prepared by a Facile Synthesis Method. *Adv. Mater.* **2012**, *24*, 2459−2462.

(8) Riedel, W.; Wiesner, S.; Greiner, D.; Hinrichs, V.; Rusu, M.; Lux-Steiner, M. C. Hybrid solar cells with ZnO-nanorods and dry processed small molecule absorber. *Appl. Phys. Lett.* **2014**, *104*, 173503.

(9) Greiner, M. T.; Helander, M. G.; Tang, W.-M.; Wang, Z.-B.; Qiu, J.; Lu, Z.-H. Universal energy-level alignment of molecules on metal oxides. *Nat. Mater.* **2012**, *11*, 76−81.

(10) Wang, Q.-K.; Wang, R.-B.; Shen, P.-F.; Li, C.; Li, Y.-Q.; Liu, L.-J.; Duhm, S.; Tang, J.-X. Energy Level Offsets at Lead Halide Perovskite/Organic Hybrid Interfaces and Their Impacts on Charge Separation. *Adv. Mater. Interfaces* **2015**, *2*, 1400528.

(11) Fleisch, T. H.; Mains, G. J. An XPS study of the UV reduction and photochromism of MoO₃ and WO₃. *J. Chem. Phys.* **1982**, *76*, 780−786.

(12) Werfel, F.; Minni, E. Photoemission study of the electronic structure of Mo and Mo oxides. *J. Phys. C: Solid State Phys.* **1983**, *16*, 6091.

(13) Soultati, A.; Douvas, A. M.; Georgiadou, D. G.; Palilis, L. C.; Bein, T.; Feckl, J. M.; Gardelis, S.; Fakis, M.; Kennou, S.; Falaras, P.; Stergiopoulos, T.; Stathopoulos, N. A.; Davazoglou, D.; Argitis, P.; Vasilopoulou, M. Solution-Processed Hydrogen Molybdenum Bronzes as Highly Conductive Anode Interlayers in Efficient Organic Photovoltaics. *Adv. Energy Mater.* **2014**, *4*, 1300896.

(14) Wong, K. H.; Ananthanarayanan, K.; Luther, J.; Balaya, P. Origin of Hole Selectivity and the Role of Defects in Low-Temperature Solution-Processed Molybdenum Oxide Interfacial Layer for Organic Solar Cells. *J. Phys. Chem. C* **2012**, *116*, 16346−16351.

(15) Vasilopoulou, M.; Douvas, A. M.; Georgiadou, D. G.; Palilis, L. C.; Kennou, S.; Sygellou, L.; Soultati, A.; Kostis, I.; Papadimitropoulos, G.; Davazoglou, D.; Argitis, P. The Influence of Hydrogenation and Oxygen Vacancies on Molybdenum Oxides Work Function and Gap States for Application in Organic Optoelectronics. *J. Am. Chem. Soc.* **2012**, *134*, 16178−16187.

(16) Greiner, M. T.; Chai, L.; Helander, M. G.; Tang, W.-M.; Lu, Z.-H. Transition Metal Oxide Work Functions: The Influence of Cation Oxidation State and Oxygen Vacancies. *Adv. Funct. Mater.* **2012**, *22*, 4557−4568.

(17) Himmerlich, M.; Koufaki, M.; Ecke, G.; Mauder, C.; Cimalla, V.; Schaefer, J. A.; Kondilis, A.; Pelekanos, N. T.; Modreanu, M.; Krischok, S.; Aperathitis, E. Effect of Annealing on the Properties of Indium−Tin−Oxynitride Films as Ohmic Contacts for GaN-Based Optoelectronic Devices. *ACS Appl. Mater. Interfaces* **2009**, *1*, 1451−1456.

(18) Dasgupta, B.; Goh, W. P.; Ooi, Z. E.; Wong, L. M.; Jiang, C. Y.; Ren, Y.; Tok, E. S.; Pan, J.; Zhang, J.; Chiam, S. Y. Enhanced Extraction Rates through Gap States of Molybdenum Oxide Anode Buffer. *J. Phys. Chem. C* **2013**, *117*, 9206−9211.

(19) Lee, K. E.; Liu, L.; Kelly, T. L. Effect of Molybdenum Oxide Electronic Structure on Organic Photovoltaic Device Performance: An X-ray Absorption Spectroscopy Study. *J. Phys. Chem. C* **2014**, *118*, 27735−27741.

(20) Liao, X.; Jeong, A. R.; Wilks, R. G.; Wiesner, S.; Rusu, M.; Bär, M. X-ray irradiation induced effects on the chemical and electronic properties of MoO₃ thin films. *J. Electron Spectrosc. Relat. Phenom.* **2016**, *212*, 50−55.

(21) Greiner, M. T.; Chai, L.; Helander, M. G.; Tang, W.-M.; Lu, Z.-H. Metal/Metal-Oxide Interfaces: How Metal Contacts Affect the Work Function and Band Structure of MoO₃. *Adv. Funct. Mater.* **2013**, *23*, 215−226.

(22) Battaglia, C.; Yin, X.; Zheng, M.; Sharp, I. D.; Chen, T.; McDonnell, S.; Azcatl, A.; Carraro, C.; Ma, B.; Maboudian, R.; Wallace, R. M.; Javey, A. Hole Selective MoOₓ Contact for Silicon Solar Cells. *Nano Lett.* **2014**, *14*, 967−971.

(23) Zhang, Z.; Xiao, Y.; Wei, H. X.; Ma, G.-F.; Duhm, S.; Li, Y.-Q.; Tang, J.-X. Impact of oxygen vacancy on energy-level alignment at MoOₓ/organic interfaces. *Appl. Phys. Express* **2013**, *6*, No. 095701.

(24) Teng, W.; Tan, X.; Li, X.; Tang, Y. Novel Ag₃PO₄/MoO₃ p-n heterojunction with enhanced photocatalytic activity and stability under visible light irradiation. *Appl. Surf. Sci.* **2017**, *409*, 250−260.

(25) Tokarz-Sobieraj, R.; Hermann, K.; Witko, M.; Blume, A.; Mestl, G.; Schlögl, R. Properties of oxygen sites at the MoO₃(010) surface: density functional theory cluster studies and photoemission experiments. *Surf. Sci.* **2001**, *489*, 107−125.

(26) Irfan; Ding, H.; Gao, Y.; Small, C.; Kim, D. Y.; Subbiah, J.; So, F. Energy level evolution of air and oxygen exposed molybdenum trioxide films. *Appl. Phys. Lett.* **2010**, *96*, 243307.

(27) Nakayama, Y.; Morii, K.; Suzuki, Y.; Machida, H.; Kera, S.; Ueno, N.; Kitagawa, H.; Noguchi, Y.; Ishii, H. Origins of Improved Hole-Injection Efficiency by the Deposition of MoO₃ on the Polymeric Semiconductor Poly(dioctylfluorene-alt-benzothiadiazole). *Adv. Funct. Mater.* **2009**, *19*, 3746−3752.

(28) Gorgoi, M.; Svensson, S.; Schäfers, F.; Öhrwall, G.; Mertin, M.; Bressler, P.; Karis, O.; Siegbahn, H.; Sandell, A.; Rensmo, H.; Doherty, W.; Jung, C.; Braun, W.; Eberhardt, W. The high kinetic energy photoelectron spectroscopy facility at BESSY progress and first results. *Nucl. Instrum. Methods Phys. Res., Sect. A* **2009**, *601*, 48−53.

(29) Schaefers, F.; Mertin, M.; Gorgoi, M. KMC-1: A high resolution and high flux soft x-ray beamline at BESSY. *Rev. Sci. Instrum.* **2007**, *78*, 123102.

(30) Shinotsuka, H.; Tanuma, S.; Powell, C. J.; Penn, D. R. Calculations of electron inelastic mean free paths. X. Data for 41 elemental solids over the 50 eV to 200 keV range with the relativistic full Penn algorithm. *Surf. Interface Anal.* **2015**, *47*, 871−888.

(31) Tanuma, S.; Powell, C. J.; Penn, D. R. Calculations of electron inelastic mean free paths. V. Data for 14 organic compounds over the 50−2000 eV range. *Surf. Interface Anal.* **1994**, *21*, 165−176.